IEEE Journal of Microwaves

Received 2 June 2022; revised 1 July 2022; accepted 28 July 2022. Date of publication 5 September 2022; date of current version 7 October 2022.

Digital Object Identifier 10.1109/JMW.2022.3195574

Detailed Analysis and Modeling of Phase Noise and Systematic Phase Distortions in FMCW Radar Systems

PETER TSCHAPEK, GEORG KÖRNER (Graduate Student Member, IEEE), CHRISTIAN CARLOWITZ (Member, IEEE), AND MARTIN VOSSIEK (Fellow, IEEE)

(Regular Paper)

Institute of Microwaves and Photonics, Friedrich-Alexander-Universität Erlangen-Nürnberg, 91058 Erlangen, Germany

CORRESPONDING AUTHOR: Peter Tschapek (e-mail: peter.tschapek@fau.de).

This work was supported in part by the Deutsche Forschungsgemeinschaft (DFG, German Research Foundation) under Grant VO 1453/33-1 and in part by Friedrich-Alexander-Universität Erlangen-Nürnberg (FAU) through funding programme "Open Access Publication Funding."

ABSTRACT In coherent continuous-wave (CW) radar systems, such as frequency-modulated CW (FMCW) radar systems, measurement precision is distorted by phase noise and systematic phase errors during radar signal generation. Unfortunately, to date, these phase distortions have typically been modeled based on many simplifications, often leading to overoptimistic predictions of radar performance. For example, phase noise is regularly considered based on additive white Gaussian noise (AWGN) models, ignoring its colored spectral property. Systematic errors are also frequently not properly separated from stochastic distortions, or not precisely measured and modeled. To overcome these issues, an advanced CW radar and frequency synthesizer model is proposed, analyzed, and experimentally verified in this paper. It is shown how systematic phase errors can be measured and how the influence of phase distortions on radar measurement can be accurately predicted. The proposed modeling approach was investigated for range correlation and range precision. The key metrics are the phase noise power spectral density (PSD) for range correlation and the variance of the frequency estimate for range precision. A 24-GHz FMCW radar system was used for the experimental verification. Long-range radar targets with distances of 38 to 880 m were created with an analog fiber optical link. Therefore, a precise and systematic evaluation of all effects was possible. The proposed phase distortion modeling approach realistically represented the range-dependent radar measurement effects. This enables the most precise simulation of and prediction for FMCW radar performance to date.

INDEX TERMS Noise analysis, noise modeling, range correlation, range precision, FMCW radar.

I. INTRODUCTION

Continuous-wave (CW) radar systems, particularly frequency-modulated (FMCW) or frequency-stepped (FSCW) systems, are widely used. These coherent systems have been established in automotive radar, industrial automation, and security and aerospace applications as wave-based sensor technology for range and velocity measurements for targets up to distances of several hundred meters. Due to the inherent signal compression and correlation in these coherent radar systems, high precision can be achieved with efficient hardware, most notably with low-bandwidth baseband signal acquisition and generation. However, the achievable precision in CW radar decreases with the range, which is caused by phase distortions occurring during the transmit (TX) signal generation. These distortions can be systematic errors, such as non-perfectly linear frequency modulation in FMCW radar, or stochastic errors, for example, caused by phase noise. Thus, the source of these errors is usually related to the frequency synthesizer. Modeling these errors is essential for radar system designers to reliably predict radar performance or specify hardware requirements. In the following, we explain that existing closed-form mathematical approaches may provide a rough estimate of phase noise–related distortions. However, these

approaches do not allow for accurate predictions due to the many simplifications required to derive the closed-form solution. Therefore, in this paper, we follow an approach based on Monte Carlo (MC) simulations.

Predicting radar performance and assessing phase distortions based on MC simulations require three steps:

1) Determining the key metrics of the systematic and stochastic synthesizer phase distortions, for example, derived with appropriate measurements.
2) Synthesizing virtual radar signals, where modulation parameters, as well as systematic and phase noise distortions, are suited to mimic all effects in the physical signal counterpart.
3) Simulating radar measurement and deriving the key metrics for radar measurement performance.

The frequency synthesizer is typically characterized by the phase noise power spectral density (PSD) [1]–[4]. The phase noise PSD of a frequency synthesizer is classically measured with commercial measuring devices and is limited to measuring unmodulated mono-frequency sinusoidal signals. Measuring the phase noise PSD during modulation is challenging and often requires sophisticated setups or is limited to specific and known modulation characteristics. Recently, in [5] an elegant approach was presented that characterizes the phase noise PSD during modulation using a differential demodulation approach to separate phase noise from systematic errors simultaneously. In the present paper, the phase distortion measurement is based on this approach.

After the frequency synthesizer is characterized, virtual radar signals can be generated. Two basic approaches are used. First, models based on the additive white Gaussian noise (AWGN) model have been established for a long time [6]–[11]. Usually, the measured phase noise PSD of a frequency synthesizer in the mono-frequency sinusoidal CW mode is converted into a single root-mean-square (RMS) phase error by integrating it over the measured spectrum. The RMS phase error is then converted into a corresponding signal-to-noise ratio (SNR) to synthesize signals based on the AWGN process.

However, to address the color property of phase noise with approximations, the power-law approaches described in [12] and [13] were used in [14] and [15] to design filter coefficients for filtering white noise in a frequency-dependent manner. In addition, in [16] the near-carrier frequency dependence was approximated with a Gaussian shape. To this end, a filter-based technique was presented in [17], in which ideally high-pass filtered white frequency noise was used to generate colored phase noise by subsequent integration. In the RMS-based approaches, the frequency-dependent information is lost with integration, while the power-law approaches are limited in their modeling by their $1/f^{\alpha}$ dependence. Furthermore, AWGN models can realistically represent reality only if the frequency synthesizer behavior is dominated by white noise.

As this is usually not the case, a second basic modeling approach based on an additive colored noise (ACN) model was developed and presented in [18]. In this new approach, the modeling of the stochastic process takes place in the frequency domain, where complete information about the frequency dependence of the phase noise PSD is used for the modeling.

The final step of modeling radar measurement addresses the estimation of performance metrics, which are often related to the achievable ranging precision. The latter can be compared with the Cramer-Rao lower bound (CRLB), which has long been established for assessing frequency and phase estimations in radar technology [6]–[10], [19], [20]. In coherent radar systems, the range-dependent correlation effect [21] of the phase noise PSD is analytically calculated for the beat signal, and the corresponding CRLB is determined. However, the CRLB approach is based on the AWGN model [22] and describes the theoretical limit of the precision of a frequency estimate. This can be expanded for different target ranges in radar technology when white noise disturbs a signal. Additionally, by considering [23], the influence of windowing on the CRLB can be corrected.

In the approaches above, systematic errors during modulation have neither been measured nor modeled. Furthermore, the approaches for describing range precision based on the CRLB or with AWGN-based simulations can be evaluated only as rough approximations and do not adequately represent the frequency synthesizer properties and their influence on radar systems.

To overcome these shortcomings, this paper combines the previous approaches for measuring phase noise during modulation in [5] and for modeling phase noise in [18]. A new method for measuring and modeling systematic errors is also presented. With the help of an MC simulation, a realistic prediction for the influence on range precision is possible for the first time. A phase noise PSD measured according to [5] and the extracted systematic errors described in this paper are required.

The remainder of the paper is organized as follows: In Section II, the model of systematic phase errors and phase noise is introduced. In Section III, the modelling of distorted oscillator signals and the resulting beat signals are described in detail. In Sections IV and V, the range correlation and range precision are analyzed, respectively. In Section VI, the combined approaches are experimentally verified in a series of measurements, and the influence of the analog fiber optical link is discussed as well as the results, followed by the conclusion.

II. MODEL OF SYSTEMATIC PHASE ERRORS AND PHASE NOISE IN FMCW RADAR

This section describes how systematic errors are separated from stochastic errors and how the underlying frequency-modulated signal is demodulated. In this work, systematic errors are defined by higher-degree polynomials.

A real-value time-limited linear frequency-modulated signal $s_{\mathrm{D}}(t)$ distorted by phase noise and systematic errors is

described by

$$s_{\mathrm{D}}(t) = \sin\left(\phi_{\mathrm{FMCW}}(t) + \sum_{n=0}^{N} x_n t^n + \phi_{\mathrm{PN}}(t)\right), \quad (1)$$

where $\phi_{\mathrm{PN}}(t)$ is the phase noise, and $\phi_{\mathrm{FMCW}}(t)$ is the ideal phase of the FMCW sinusoidal signal. Due to time limitations, the phase noise $\phi_{\mathrm{PN}}(t)$ is high-pass band-limited and can be considered wide-sense stationary [24]. The systematic errors are described by an N-degree polynomial, with N as the order and x_n as the polynomial coefficients. The ideal phase $\phi_{\mathrm{FMCW}}(t)$ of the FMCW sweep is given by [25]

$$\phi_{\mathrm{FMCW}}(t) = \sum_{n=0}^{2} y_n t^n = \phi_0 + \omega_0 t + \frac{1}{2}\mu t^2, \quad (2)$$

where ϕ_0 is the starting phase, $\omega_0 = 2\pi f_0$ is the angular frequency, f_0 is the frequency, y_n are the coefficients of the second-degree polynomial, and μ is the sweep rate with

$$\mu = \frac{2\pi B_{\mathrm{S}}}{T_{\mathrm{S}}}, \quad (3)$$

where B_{S} is the bandwidth, and T_{S} is the sweep time of the sweep. A generalized version of the phase $\phi_{\mathrm{D}}(t)$ of the distorted signal in (1) can be written as

$$\phi_{\mathrm{D}}(t) = \sum_{n=0}^{N} z_n t^n + \phi_{\mathrm{PN}}(t), \quad (4)$$

where

$$z_n = x_n + y_n. \quad (5)$$

It is evident that the ideal FMCW sweep $\phi_{\mathrm{FMCW}}(t)$ in (2) described by a second-degree polynomial of the ideal sweep was merged with the N-th degree polynomial of the systematic error in (1) to create a common polynomial with common coefficients described by z_n. This is because in reality the two polynomials cannot be separated from each other without a priori knowledge.

If the signal in (1) is the result of a stochastic process, the signal is to be considered a realization $s_{i,\mathrm{D}}(t)$ of the process. The process is considered cyclostationary with regard to the sweep length, which corresponds to the sweep time T_{S}. Therefore, the following assumptions can be made. First, the systematic errors, and therefore the coefficients of the polynomial, are invariant from realization to realization. These relationships result in

$$z_{i,n} = z_{i-1,n}. \quad (6)$$

Second, the statistical properties of the phase noise $\phi_{\mathrm{PN}}(t)$ are invariant for an integer time shift over bT_{S}, and averaging the phase noise $\phi_{\mathrm{PN}}(t)$ over the realizations leads to

$$\frac{1}{M}\sum_{1}^{M} \phi_{i,\mathrm{PN}}(t) \approx 0, \quad (7)$$

where M is the number of realizations. With the model of the phase $\phi_{\mathrm{D}}(t)$ in (4) of a distorted FMCW signal, the presence of a stochastic process, and the assumptions made in (6) and (7), the systematic errors can now be defined and extracted.

To separate the systematic errors of the signal, averaging of the unwrapped distorted phase $\phi_{\mathrm{D}}(t)$ is calculated according to

$$\bar{\phi}_{\mathrm{D}}(t) = \frac{1}{M}\sum_{1}^{M} \phi_{i,\mathrm{D}}(t) = \sum_{n=0}^{N} z_n t^n. \quad (8)$$

The phase noise, $\phi_{\mathrm{PN}}(t)$, which is the stochastic part of the signal, is lost through averaging regarding the assumption in (7). A second-degree polynomial fit p_2 of the averaged phase $\bar{\phi}_{\mathrm{D}}(t)$ results in

$$\phi_{\mathrm{p2}}(t) = p_2\left(\bar{\phi}_{\mathrm{D}}(t)\right) = \sum_{n=0}^{2} z_n t^n. \quad (9)$$

Then, the demodulation is performed by subtracting $\phi_{\mathrm{p2}}(t)$ from $\bar{\phi}_{\mathrm{D}}(t)$, and the higher-degree systematic errors $\phi_{\mathrm{SYS}}(t)$ can be defined as

$$\phi_{\mathrm{SYS}}(t) = \bar{\phi}_{\mathrm{D}}(t) - \phi_{\mathrm{p2}}(t) = \sum_{n=3}^{N} x_n t^n. \quad (10)$$

The time-dependent bandlimited phase noise $\phi_{\mathrm{PN}}(t)$ is modeled according to [18]. The colored properties of phase noise are considered, and arbitrary realizations of phase noise with identical statistical properties can be generated with a stochastic process. The resulting modeling process can be described by the function f_{PN}

$$\phi_{\mathrm{PN}}(t) = \phi_{\mathrm{PN}}\left(t,\, \mathscr{L}\right) = f_{\mathrm{PN}}\left(t, \mathscr{L}_{\mathrm{FMCW}}(f)\right), \quad (11)$$

where the necessary phase noise (PSD) $\mathscr{L}_{\mathrm{FMCW}}(f)$ during an FMCW sweep is measured and extracted according to [5].

For the modeling of systematic errors, measured FMCW sweeps in the baseband, as described in [5], are used to extract the higher-degree polynomial systematic errors according to the derivation above. The processing can be described as a function, where the phase of a measured FMCW sweep $\phi_{\mathrm{D}}(t)$ is an argument. This results in

$$\phi_{\mathrm{SYS}}(t) = f_{\mathrm{SYS}}(\phi_{\mathrm{D}}(t)). \quad (12)$$

III. MODELING OF FMCW RADAR BEAT SIGNALS

In this section, the modeling of FMCW radar signals distorted by phase noise and systematic errors is described. Then, a conventional monostatic primary FMCW radar system is used with a single static target, which is illustrated in Fig. 1, to model FMCW radar beat signals.

Starting from a time-limited transmit signal, the beat signal is derived as a function of the target range. The influence of different backscatter cross-sections, as well as the reduction of the amplitude for targets far away as a result of the free-space path loss, are not considered.

Based on the equation described in Section II, a realistic oscillator phase model that contains systematic phase errors

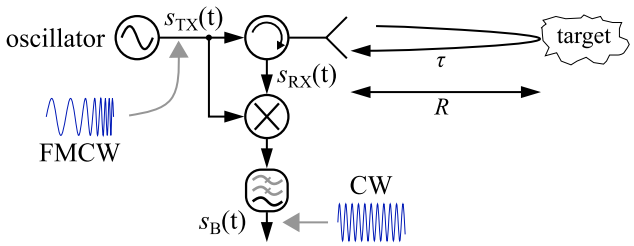

FIGURE 1. Schematic representation of the principle of a monostatic primary FMCW radar system as a block diagram with a single static target.

and phase noise can be derived as

$$\phi_D(t) = \phi_0 + \omega_0 t + \frac{1}{2}\mu t^2 + \phi_{SYS}(t) + \phi_{PN}(t). \tag{13}$$

In Fig. 1, the transmit signal $s_{TX}(t)$ of an FMCW radar signal, which is distorted by phase noise and systematic errors, according to (13) is defined as

$$s_{TX}(t) = \sin\left(\phi_0 + \omega_0 t + \frac{1}{2}\mu t^2 + \phi_{SYS}(t) + \phi_{PN}(t)\right), \tag{14}$$

where the phase noise can be considered wide-sense stationary due to time limitations. The target at a range of R results in a propagation delay τ of the received signal $s_{RX}(t)$. At the mixer, the transmit signal $s_{TX}(t)$ and the received signal $s_{RX}(t)$ are mixed to the beat signal. The resulting phase of the low-pass filtered beat signal $s_B(t)$ is valid for $\tau \ll T_S$ and $2\pi B_S \ll \omega_0$. The resulting phase of the filtered beat signal can be written as

$$\phi_{B,PN+SYS}(t) = \omega_0\tau + \mu\tau t + \phi_{SYS}(t) - \phi_{SYS}(t-\tau) + \phi_{PN}(t) - \phi_{PN}(t-\tau), \tag{15}$$

which is distorted by phase noise and systematic errors in the transmit signal. If we consider only the beat signal, which is distorted by phase noise, then the phase of the beat signal can be rewritten as

$$\phi_{B,PN}(t) = \omega_0\tau + \mu t\tau + \phi_{PN}(t) - \phi_{PN}(t-\tau). \tag{16}$$

IV. ANALYSIS OF RANGE CORRELATION

In this section, we analyze the correlation effect occurring in the beat signal due to the colored property of the phase noise and the coherent principle of the radar, as shown in Fig. 1.

A. CLOSED-FORM ANALYSIS

The range correlation can be analyzed using a closed analytical solution according to [21] and results in

$$\mathcal{L}_{B,PN}(f, R, \mathcal{L}) = \mathcal{L}_{FMCW}(f)\left(2 - 2\cos\left(\frac{4\pi R f}{c_0}\sqrt{\varepsilon_r}\right)\right), \tag{17}$$

where $\mathcal{L}_{FMCW}(f)$ is the measured phase noise PSD of the transmit signal during an FMCW sweep measured according to [5], ε_r is the relative permittivity of the propagation medium, f is the relative frequency range to the carrier frequency, and $\mathcal{L}_{B,PN}(f, R, \mathcal{L})$ is the resulting range-correlated phase noise PSD of the beat signal. The resulting phase noise PSD $\mathcal{L}_{B,PN}(f, R, \mathcal{L})$ is formed around the beat frequency and depends on the target range R and the underlying phase noise PSD $\mathcal{L}_{FMCW}(f)$ of the transmit signal.

B. MONTE CARLO ANALYSIS

The analytically calculated phase noise PSD $\mathcal{L}_{B,PN}(f, R, \mathcal{L})$ in (17) can also be determined with MC simulations. In [18], a method was presented that allows the modeling of phase noise based on a measured phase noise PSD $\mathcal{L}$, where the colored property of the phase noise is preserved. This modeling can be described by a function according to (11), and the resulting phase noise is generated by an MC simulation. The calculated beat signal in (16) distorted by the modeled and simulated phase noise according to (11) can be demodulated using the method presented in [5]. To bring out the dependencies of the beat signal clearly, (16) can be rewritten as a function such as

$$\phi_{B,PN}(t) = f_B\left(R,\ \phi_{PN}\left(t, \mathcal{L}_{FMCW}\right)\right), \tag{18}$$

where the phase of the beat signal depends on the target range R and the modeled phase noise ϕ_{PN}, which depends on the measured phase noise PSD $\mathcal{L}$. The phase noise PSD $\mathcal{L}_{B,PN}(f, R, \mathcal{L})$ of the resulting phase of the beat signal distorted by wide-sense stationary phase noise can be obtained based on the Wiener-Khinchine theorem using (18) and the Fourier transform (FT) with

$$\mathcal{L}_{B,PN}(f, R, \mathcal{L}) = \frac{1}{T}\left\langle \left| \int_0^T f_\phi\left(\phi_{B,PN}(t)\right) e^{-j\omega t} dt \right|^2 \right\rangle_M, \tag{19}$$

where T is the signal length, M is the number of realizations, and the function $f_\phi(\phi(t))$ demodulates the phase according to [5]. In (19), the averaging of the M PSD was performed because, as is well-known, the PSD is an inconsistent estimator, and variance is reduced only by averaging while maintaining the spectral resolution.

C. METRICS AND RESULTS

The results of the analytical analysis according to (17) and the MC analysis according to (19) are shown in Fig. 2. The PSD shown in Fig. 2 is used as a metric to compare the two analysis approaches. The phase noise PSD of the beat signals of the target range $R = 38$ m and $R = 407$ m are presented. The drawn phase noise PSD $\mathcal{L}_{FMCW}$ was used for analytical and MC modeling, which has been measured using the setup shown in [5] with the following parameters of the frequency synthesizer: $B_S = 100$ MHz, $T_S = 1$ ms, and $f_0 = 24.1$ GHz.

For the MC simulation, the phase noise PSD $\mathcal{L}_{FMCW}$ was linearly interpolated to obtain equally distributed frequency points on the spectrum. The sampling frequency of the simulation was chosen as $f_S = 2$ GHz. The simulated beat signals were down-sampled by a factor of 2^6 to a sampling frequency

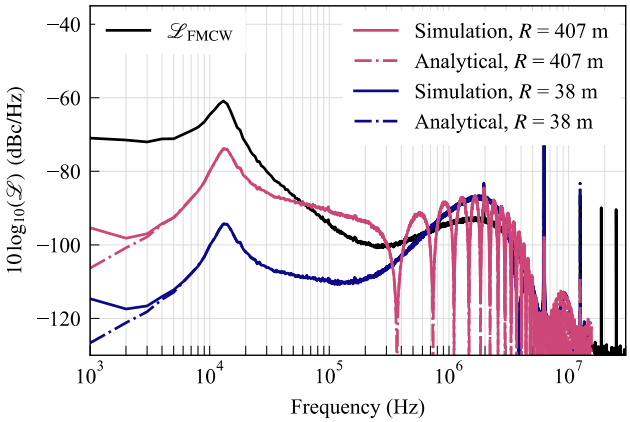

FIGURE 2. Analysis and comparison of the range correlation effect for two different target ranges based on the phase noise PSD of the respective beat signals for the analytical and simulative approaches.

of 31.25 MHz. The averaging of the spectrum of the beat signal is the result of 2000 runs during the MC simulation.

In the plots in Fig. 2, we can see very good agreement between the analytical and simulative approaches for both ranges. At higher frequencies, we see a collapse in the spectrum at the frequency points with integer multiples of $1/\tau = c_0/2R$, where the most complete cancellation of phase noise in the spectrum can be seen there. This is because the mixing of two temporally shifted signals due to the transit time in a radar system corresponds to the convolution in the frequency domain. The convolution leads to the correlation of the signals, which is highest when the signals are shifted by the factor of integer multiple of τ as a result of the convolution.

V. ANALYSIS OF RANGE PRECISION

In this section, the metric used to describe the range-dependent range precision is introduced. Then, the individual effects that have a significant impact on the range precision are presented, analyzed, and compared regarding their importance for the range precision prediction.

A. ANALYSIS METRIC

In the classical FMCW radar system, the range R of a single target is proportional to the beat frequency f_{Beat} of the beat signal and can be written as

$$R = \frac{c_0 T_{\mathrm{S}}}{2B_{\mathrm{S}}} f_{\mathrm{Beat}}, \tag{20}$$

where f_{Beat} is detected as the frequency of the maximum peak in the spectrum of the beat signal. The spectrum was calculated using the discrete Fourier transform (DFT). In reality, the ideal beat frequency f_{Beat} in (20) is affected by stochastic signal components in the beat signal, which leads to an imprecise range estimation. Each stochastic signal is the result of a stochastic process based on probability distributions. As the exact probability distributions are often unknown, statistical moments are used. This is possible because without knowledge about the probability distribution, these moments offer the possibility to describe and quantify the influence of stochastic signal components on range precision. In general, systematic errors influence the accuracy, and random errors influence the precision of a measurement [26]. A generic approach to quantifying the precision of the frequency estimate of the beat frequency represents the standard deviation, which is the root of the second central moment and is defined by

$$\sigma(f_{\mathrm{Beat}})|_M = \sqrt{\frac{1}{M}\sum_{m=1}^{M}\left(\hat{f}_{\mathrm{Beat},m} - \bar{f}\right)^2}, \tag{21}$$

where $\hat{f}_{\mathrm{Beat},m}$ is the current estimated beat frequency of the m-th realization of the stochastic process, and $\bar{f}$ is the sample mean of the frequency estimate of M realizations. In (21), wide-sense stationarity is assumed, and beat signals are time-limited realizations of the stochastic process. This allows us to specify the precision of the range according to (20) and (21):

$$\sigma(R)|_M = \frac{c_0 T_{\mathrm{S}}}{2B_{\mathrm{S}}}\sigma(f_{\mathrm{Beat}})|_M. \tag{22}$$

B. IMPACT OF SYSTEMATIC ERRORS AND PHASE NOISE

The range precision can now be expressed mathematically for beat signals distorted by phase noise. Equation (16) defines the corresponding phase of the beat signal. With the time-derivative of the bandlimited phase, the beat frequency at maximum is defined as

$$\begin{aligned} f_{\mathrm{B,PN}} &= \frac{1}{2\pi}\frac{\mathrm{d}\phi_{\mathrm{B,PN}}(t)}{\mathrm{d}t} \\ &= \frac{\mu\tau}{2\pi} + \frac{\mathrm{d}\left[\phi_{\mathrm{PN}}(t) - \phi_{\mathrm{PN}}(t-\tau)\right]}{2\pi\,\mathrm{d}t}. \end{aligned} \tag{23}$$

The corresponding range precision for a single target at a target range of R is calculated according to (22) as follows:

$$\sigma_{\mathrm{PN}}(R)|_M = \frac{c_0 T_{\mathrm{S}}}{2B_{\mathrm{S}}}\sigma\left(f_{\mathrm{B,PN}}\right)\big|_M. \tag{24}$$

Similarly, the beat frequency can be expressed mathematically when the bandlimited phase of the beat signal in (15) is affected by phase noise and systematic errors. This beat frequency is defined as

$$\begin{aligned} f_{\mathrm{B,PN+SYS}} = \frac{\mu\tau}{2\pi} &+ \frac{\mathrm{d}\left[\phi_{\mathrm{SYS}}(t) - \phi_{\mathrm{SYS}}(t-\tau)\right]}{2\pi\,\mathrm{d}t} \\ &+ \frac{\mathrm{d}\left[\phi_{\mathrm{PN}}(t) - \phi_{\mathrm{PN}}(t-\tau)\right]}{2\pi\,\mathrm{d}t}. \end{aligned} \tag{25}$$

Furthermore, the corresponding range precision for a single target at a target range of R is calculated according to (22) as follows:

$$\sigma_{\mathrm{PN+SYS}}(R)|_M = \frac{c_0 T_{\mathrm{S}}}{2B_{\mathrm{S}}}\sigma\left(f_{\mathrm{B,PN+SYS}}\right)\big|_M. \tag{26}$$

As can be seen in (25), in this work, systematic errors are modeled in the transmit signal $s_{\mathrm{TX}}(t)$ and not in the beat signal. Therefore, due to the radar principle, the systematic errors in the signals occurring at the mixer are shifted over time. As a result, the frequency spacing of the instantaneous

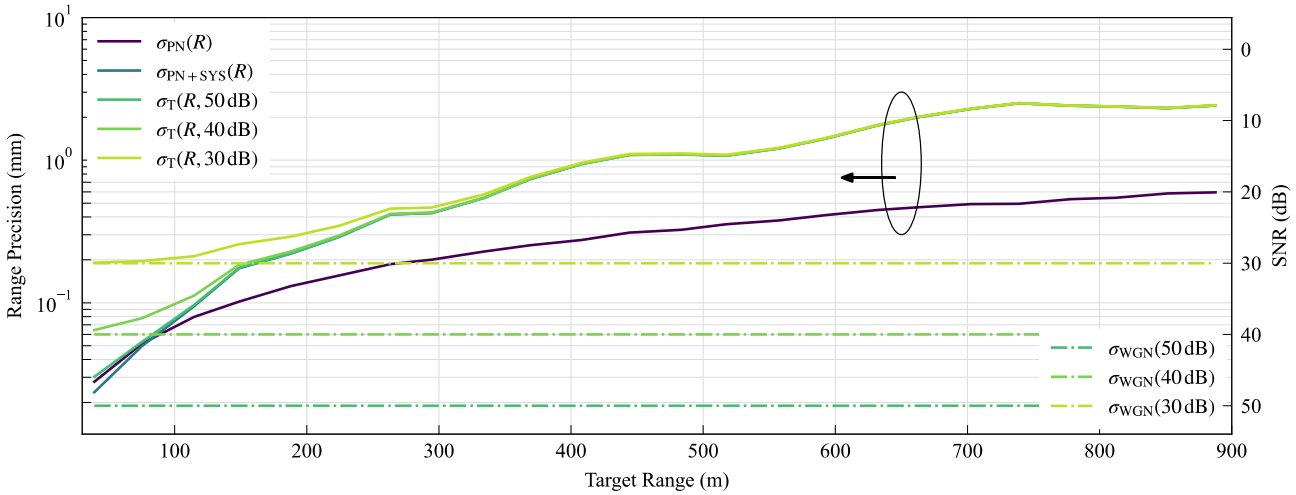

FIGURE 3. Comparison of the range precision as a function of the target range for different models. The right ordinate additionally shows the SNR corresponding to the range precision, which is used for models with WGN.

frequencies was not constant during the sweep. This leads to a broadening of the main lobe of the beat frequency in the spectrum. Thus, systematic errors not only influence the accuracy but, in the case of a radar system, also have a direct influence on the precision of the frequency estimate in the beat signal.

C. WHITE GAUSSIAN NOISE

If white noise is present in a radar system, the detectability of targets is limited not by the radar principle but primarily by the receiver chain. In general, the beat signals can be brought into the required level range with a higher output power in the transmit signal, by a lower noise figure (NF) of low noise amplifiers (LNAs) in the receiver chain. The white Gaussian noise floor in the transmit signal can increase considerably due to the transmission channel or the receiver chain. The SNR is more independent of the source of noise.

The precision with which a target can be detected when white noise dominates depends on the SNR. The influence of white Gaussian noise on the frequency estimation can be approximated with the CRLB [22]. Therefore, the range precision is defined as

$$\sigma_{\mathrm{WGN}}(\mathrm{SNR}) = \frac{c_0 T_S}{2B_S}\sqrt{\frac{12 f_S^2}{4\pi^2 N^3 \mathrm{SNR}}}\, k_{\mathrm{WIN}}, \tag{27}$$

where N is the number of samples, f_S is the sampling frequency, and k_{WIN} describes the degradation of the precision due to the windowing [23].

As the purpose of this work is to investigate the precision of the frequency estimation of a radar system that is primarily influenced by phase noise, a high dynamic range is required for experimental validation of the phase noise influence. This means that the SNR of the receiver output in the measurement setup must be as high as possible. Residual system-related white noise, which has an influence on the range precision as described in (27), must be modeled accordingly.

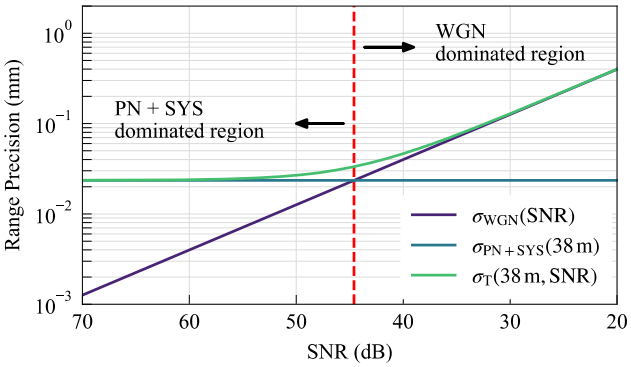

FIGURE 4. Precision of range estimation as a function of the SNR in the presence of WGN for a single target at the range of $R = 38$ m. The threshold, which is marked as the dashed red line, was determined at an SNR of 44.6 dB.

D. OVERALL RANGE PRECISION

The root of the squared range precision in (26) and (27) describes the total influence of phase noise, systematic errors, and white Gaussian noise and can be written as

$$\sigma_{\mathrm{T}}(R, \mathrm{SNR})|_M = \sqrt{\sigma^2_{\mathrm{PN+SYS}}(R)\big|_M + \sigma^2_{\mathrm{WGN}}(\mathrm{SNR})}. \tag{28}$$

E. OVERALL RESULTS OF THE ANALYSIS

The results of the MC simulation for range precision analysis are shown in Figs. 3 and 4. For the modeling of phase noise, the phase noise PSD $\mathscr{L}_{\mathrm{FMCW}}$, which is shown in Fig. 2, was used. In this regard, the phase noise PSD is linearly interpolated to obtain equally distributed frequency points.

The systematic errors were extracted from the measured FMCW sweeps in the baseband according to the derivation in Section II, which were used for the plot of the phase noise PSD $\mathscr{L}_{\mathrm{FMCW}}$ in Fig. 2. The simulated FMCW sweeps were generated in the baseband from 100 to 200 MHz with

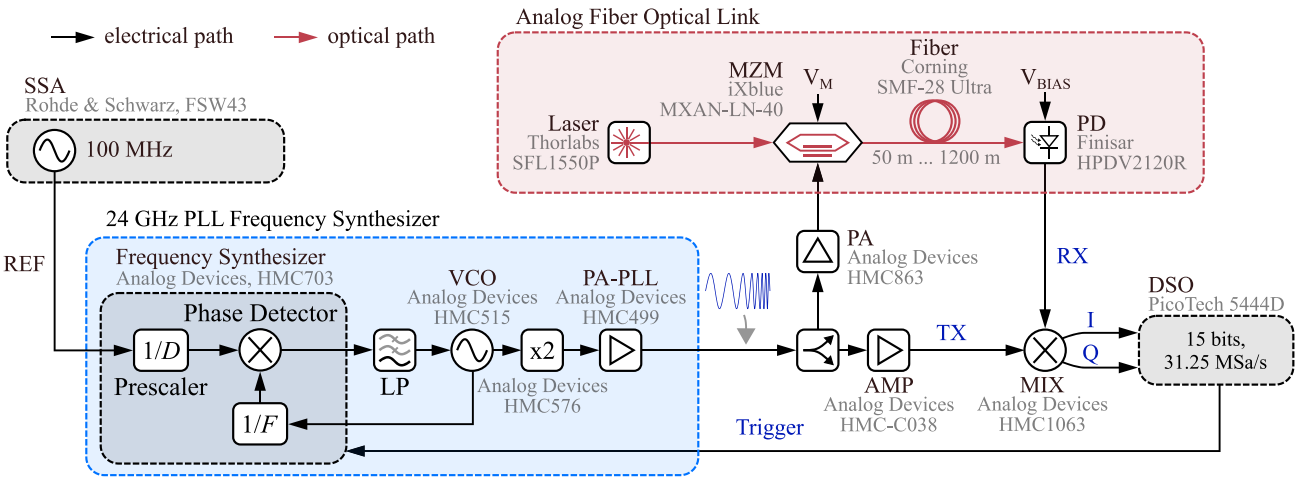

FIGURE 5. Experimental verification setup. Electrical signals are marked by black arrows and optical signals by red arrows. The signal designations are in blue.

1 ms sweep time. The MC simulation for modeling the range precision was performed on the transmit side with a sampling frequency of 2 GHz, and the simulated beat signals were down-sampled on the receiver side by a factor of 2^6 to 31.25 GHz. In total, 24 ranges with 2000 runs per analyzed target range from 38 to 880 m were simulated. The distance between the simulated ranges was approximately 38 m. During the digital signal processing (DSP) of the simulated beat signals, the signals were filtered through a Hamming window and transformed into the frequency domain using DFT and with zero padding of factor 8. The beat frequency was determined with a parabolic peak fit. For this analysis, the SNR was assumed to be independent of the range.

Starting with Fig. 3, we see the simulated precision plotted on the left ordinate axis as a function of the range of the target for different transmit signal models. It can be clearly seen that phase noise and systematic errors dominate the precision of the frequency estimation with an increasing target range. A decrease in the SNR has the dominant influence, especially for short-range targets thus, phase noise or systematic errors can be neglected in this case. The SNR underlying the white Gaussian noise (WGN) and the resulting precision in the range estimation are plotted on the right ordinate axis. The two ordinate axes can be converted into each other via (27). It can be clearly seen that in this simulated scenario, the precision is strongly range-dependent.

In comparison, Fig. 4 shows the range precision as a function of the SNR at a constant target range of 38 m. The SNR of the WGN varies from 20 to 70 dB. Thus, the term in (28) is dominated by phase noise and systematic errors and WGN in two distinguishable regions. As the SNR decreases, the range precision decreases, and the WGN dominates. At a higher SNR, the phase noise and systematic errors dominate. The threshold between the two regions in this scenario is at an SNR of 44.6 dB, which is the point where they have the same influence.

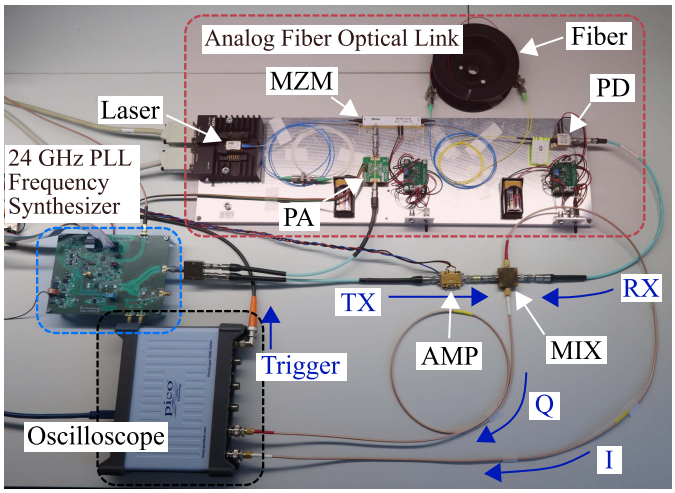

FIGURE 6. Experimental verification implementation.

VI. EXPERIMENTAL VERIFICATION

The concept and the measurement setup are presented in this section. To reproduce such large ranges reliably under laboratory conditions, an analog fiber optical link was used. Its properties and influence are discussed, followed by the results of the measurements of the range correlation and the range precision.

A. SETUP AND CONCEPT

For the experimental verification of the models, the setup shown in Figs. 5 and 6 was used. The core of this work is the modeling of distortions caused by phase noise and systematic errors. To realize the intended ranges of up to several hundred meters and to decouple the influence of the low SNR in setups with high attenuation, an analog fiber optical link as a transmission channel was used to design a system that realizes

large time delays with low attenuation. The concept is shown in detail in Fig. 5.

The system is a primary 24-GHz FMCW radar system with synthetic targets consisting of a 24-GHz phase-locked-loop (PLL) frequency synthesizer, an analog fiber optical link, a digital sampling oscilloscope (DSO, PicoScope 5444D), and various radio frequency (RF) modules. The 24-GHz PLL frequency synthesizer generates FMCW radar signals from 24.1 GHz to 24.2 GHz with a sweep time of 1 ms and a sweep repetition interval of 2.5 ms. At the output of the 24-GHz PLL frequency synthesizer, the generated radar signal is split into a direct (TX) path and a delayed (RX) path via a power splitter. The signal in the RX path is amplified by a power amplifier (PA, Analog Devices HMC863) and modulated via a Mach-Zehnder modulator (MZM, iXblue MXAN-LN40) on an optical carrier with a wavelength of $\lambda = 1550\,\text{nm}$ by intensity modulation. The MZM operates at the quadrature point. The signal of the optical carrier is provided by a single-frequency laser (Laser, Thorlabs SFL1550P). The length of the single-mode fibers (SMF, Corning SMF-28 Ultra) defines the desired target range, in which the refractive index of the fiber of $n = 1.4682$ must be considered. At the photodetector (PD, Finisar HPDV2120R), the signal is converted back into the electrical domain and is available as an RX signal at the in-phase and quadrature (IQ) mixer (MIX, Analog Devices HMC1063).

In parallel, the transmit signal via the TX path is amplified (AMP, HMC-C038) and supplied to the MIX as a local oscillator (LO). The transmit signal via the TX path and the receive signal via the RX path are mixed at the MIX, and the resulting beat signal is detected via the DSO as a complex-valued beat signal. The DSO operates with a vertical resolution of 15 bits and a sample rate of 31.25 MSa/s for each channel. The start time of the FMCW sweeps provided by the 24-GHz PLL frequency synthesizer are triggered by the DSO.

The 24-GHz PLL frequency synthesizer was developed at our institute and allows the generation of FMCW sweeps at 24 GHz with different phase noise PSD profiles during the sweep. The PLL feedback loop consists of a frequency synthesizer (Analog Devices HMC703) with a phase detector, a low-pass filter (LP), and a voltage-controlled oscillator (VCO, Analog Devices HMC515). The output signal of the VCO is multiplied by a factor of two with an active frequency multiplier (Analog Devices HMC576) and amplified to 14 dBm output power at a power amplifier (PA-PLL, Analog Devices HMC499). The output of a highly stable reference oscillator of a signal and source spectrum analyzer (SSA, Rohde & Schwarz FSW43) provides a 100 MHz reference clock with $\mathscr{L}(1\text{ kHz}) < -155\,\text{dBc/Hz}$.

The prescaler has a direct influence on the PLL transfer function during an FMCW sweep. By choosing a different prescaler D in the reference path before the phase detector, the two different phase noise PSD profiles (A) and (B) can be synthesized. The selected prescaler values are listed in Table 1. It should be emphasized that better phase noise, transient response and higher SNR can be achieved by optimizing the loop filter and charge pump. However, this is not necessary in the context of this work, since only the generation of different PSD profiles is important. In this respect, the properties of the PLL, such as loop filter or charge pump, are unchanged for both profiles. The synthesized phase noise PSD profiles were measured using the method presented in [5] and are shown in Fig. 7. The systematic errors associated with the phase noise PSD profiles (A) and (B) shown in Fig. 7, which were described in Section II, are shown in Fig. 8.

The DSP of the measured beat signals is identical to the analysis of the simulated beat signals described in Sections IV and V. Within the scope of a series of measurements, 2000 measurements were performed within 5 s for each installed fiber length. The measurements for each synthetic target range (emulated via different fiber lengths) were repeated in intervals of 50 m from 50 m to 1200 m. Subsequently, the

TABLE 1. PLL Prescaler Parameter for FMCW Radar Signal Generation Using a 24-GHz PLL Frequency Synthesizer

Name	D	F_{Start}	F_{Stop}
(A)	4	120.5	121.0
(B)	16	482.0	484.0

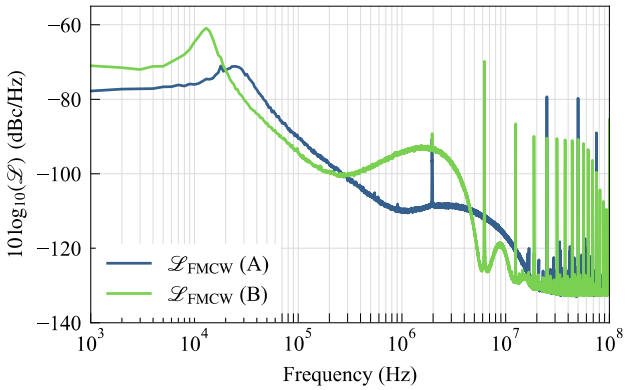

FIGURE 7. Characterization of the two different measured phase noise PSD profiles during an FMCW sweep.

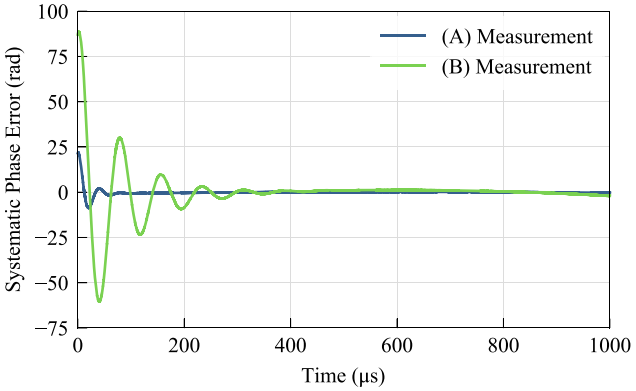

FIGURE 8. Characterization of the measured systematic errors for two different phase noise PSDs during an FMCW sweep.

TABLE 2. Parameter of the Components of the Analog Fiber Optical Link

Component	Parameter	Value
Laser	T_{TEC}	27.25 °C
	I_{Laser}	375 mA
	P_{Laser}	59 mW
MZM	V_{M}	0.25 V
PD	V_{BIAS}	4 V

beat signals sampled at 31.25 MSa/s were demodulated for the range correlation using the method described in [5], and the phase noise PSD was calculated. For this purpose, the phase noise PSD profiles shown in Fig. 7 were set at the 24-GHz PLL frequency synthesizer. For the range precision, the signals of the phase noise PSD profiles (A) and (B) were measured and evaluated. The measured beat signals were filtered through a Hamming window and transformed into the frequency domain using DFT and with zero padding of factor 8. The beat frequency was determined with a parabolic peak fit.

B. ANALOG FIBER OPTICAL LINK

Noise can be added to the microwave signal by the analog fiber optical link. A distinction must be made between noise contributions that increase either the noise floor far from the carrier by adding white Gaussian noise or the phase noise of the RF signal close to the carrier by adding colored noise.

The first case, where additional white Gaussian noise increases the noise floor and reduces the SNR, has been sufficiently researched, and its influence can be modeled and measured [27]–[29]. To exclude this influence, low-noise components were selected, and the system was operated in a controlled low-noise operating point. For this purpose, a laser with relative intensity noise (RIN) lower than –150 dB/Hz was selected, and the temperature of the laser was controlled by a thermoelectric cooler (TEC) and the laser current by a laser diode (LD) controller. With the laser parameters given in Table 2, a side mode suppression ratio (SMSR) of 53 dB was realized. The intrinsic losses were reduced to a minimum of 24 dB due to the high optical laser output power of 59 mW and the operation of the MZM at the quadrature point. Intrinsically low losses of the optical link reduced the NF [28]. With these parameters, the NF was determined by measurement to 51.3 dB using the commercial signal and source analyzer (FSW43, Rohde & Schwarz) with integrated NF measurement.

The second case, where the phase noise of the microwave signal is increased, can occur only if two conditions are satisfied. First, there must be sources of low-frequency colored noise (e.g., 1/f noise) terms, and second, there must be nonlinear processes in the analog fiber optical link that can fold these low-frequency components around the microwave signal. The sources can be the laser, the fiber, or the PD. Due to the relatively low optical power of less than 60 mW and

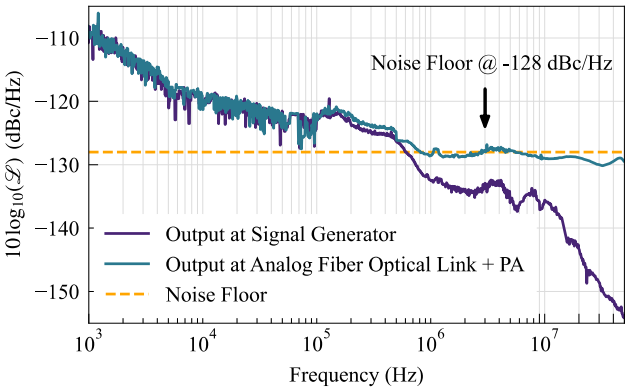

FIGURE 9. Comparison of phase noise at the output of the SG and at the output of the component chain consisting of the AMP and the analog fiber optical link. The noise floor at the output is shown with the orange dash line.

the relatively short fiber length of up to 1.2 km, no additional noise quantities are to be expected from the fiber [30]. Thus, Rayleigh scattering, stimulated Brillouin scattering, and frequency modulation (FM) to phase modulation (PM) conversion by dispersion of the fiber can be neglected. Instead of a balanced PD, a high-power PD was used, in which the 1/f noise of the laser source dominated the 1/f noise of the PD [30]. This means that in this system, only the laser has to be considered a noise source.

The dominant nonlinear device in the analog fiber optical link is the PD, because the nonlinearities of the MZM and the fiber are negligible at low optical powers [31]. The nonlinearity of the PD occurs because the propagation speed of the signal in the semiconductor depends on the number of carriers in the semiconductor material, where the number of carriers is proportional to the quadratic of the optical input power [27]. As a result of the fluctuations in the optical power caused by RIN, the colored low-frequency RIN, which shows a 1/f dependency close to the optical carrier at 1550 nm, is converted to excess phase noise at the PD [31]–[33].

Therefore, the RIN-to-phase noise conversion in the PD is the only influence to be investigated. The results of the phase noise measurement are shown in Fig. 9, which were measured with a highly sensitive cross-correlation-based phase noise analyzer (PNA, AnaPico APPH20G). The phase noise at the output of a low phase noise signal generator (SG, Rohde & Schwarz SMA100B) in the mono-frequency sinusoidal CW mode at 24 GHz was compared with the phase noise at the output of the component chain consisting of the PA and analog fiber optical link, where the SG was used as the input signal at the PA. The analog fiber optical link was operated with the parameters listed in Table 2.

In Fig. 9, two effects are visible. First, no additional phase noise is visible through the analog fiber optical link system up to a 200 kHz offset frequency above the phase noise of the SG. From about 600 kHz, a pronounced noise floor at –128 dBc/Hz is visible. Thus, the SNR at the output of the analog fiber optical link corresponding to the noise floor can

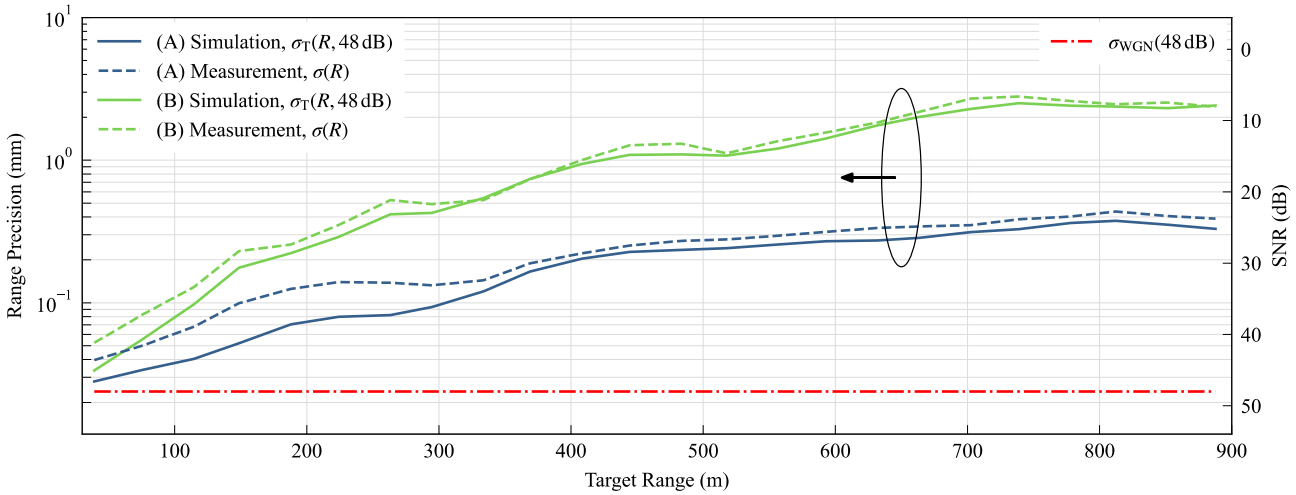

FIGURE 10. Results for the range precision measurement of the phase noise PSD profiles (A) and (B).

TABLE 3. Properties of the Overall Analog Fiber Optical Link

Parameter	Value
Loss	24.0 dB
Noise Figure	51.3 dB

be determined to be 50 dB, according to [6]. If the SNR is higher than the quantization noise at the DSO, the noise floor due to the analog optical fiber link can be neglected.

Furthermore, due to the short measurement time of 5 s per range, temperature-related expansion effects or the change in the refractive index and the associated change in propagation time through fiber can also be neglected. The phase noise of the optical carrier, quantified over the linewidth of the laser, correlates at the PD with realizations of itself, and thus does not contribute to the phase noise of the electrical signal. The input power of the MZM was configured to a maximum of 14 dBm, below the 1 dB compression point of about 17 dBm to prevent nonlinearity during the intensity modulation.

In summary, the analog fiber optical link shown in Figs. 5 and 6 operated with the parameter listed in Table 2 and the measured properties in Table 3 is considered a linear attenuating two-port network with a defined time delay. Thus, the influence on the precision of the distance estimation is negligible.

C. SENSITIVITY

The SNR at the output of the 24-GHz PLL frequency synthesizer was determined to be larger than 87 dB. The subsequent signal chain consisting of the power splitter, PA, analog fiber optical link, and MIX had a total NF of 36 dB with a common loss of 28 dB. Thus, the remaining SNR at the DSO was at least 51 dB. The quantization noise at the detector, considering the amplitude of the beat signals, had a measured maximum of 48 dB. Therefore, the quantization noise dominated the SNR of the signal and was considered the central source of white Gaussian noise.

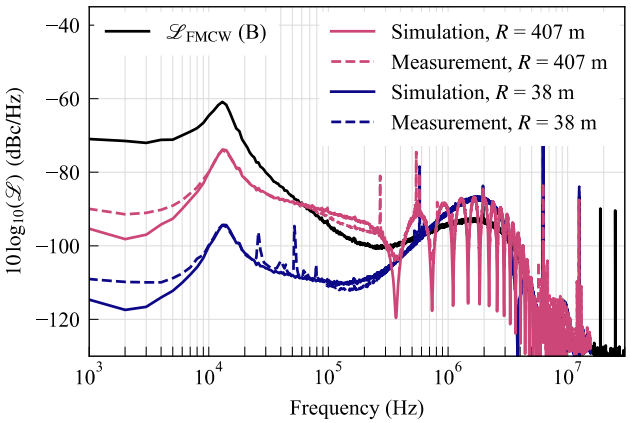

FIGURE 11. Results for the range correlation of the phase noise PSD (B) for the two different ranges. The measured results are compared with the simulated phase noise PSD.

D. RANGE CORRELATION RESULTS

In Fig. 11, the results of the range correlation of the phase noise PSD (B) for the target range of 38 and 407 m are shown. The phase noise PSD was calculated from the measured beat signals according to the procedure in [5] and compared with the phase noise PSD of the simulated beat signals in the desired range. For both ranges, from about a 7-kHz offset frequency, the curves overlap well. As explained in the analysis section, and as can be seen in Fig. 2, the dips in the spectrum are also due to the time delay of the target range.

E. RANGE PRECISION RESULTS

In Fig. 10, the results of the range precision measurements are compared with the simulated results. For the simulation, the phase noise PSD profiles of (A) and (B) shown in Fig. 7

and the corresponding systematic errors shown in Fig. 8 were used. In addition, an SNR of 48 dB was assumed to represent the influence of quantization noise. (28) describes the corresponding model for the overall simulated range precision. The measurements were performed according to the setup in Figs. 5 and 6, where the 24-GHz PLL frequency synthesizer synthesized the FMCW sweeps in a series of measurements with 2000 runs. In the figure, the range precision is plotted on the left ordinate. The corresponding SNR of the range precision for the WGN processes is plotted on the right ordinate. Both simulated curves of the range-dependent precision agree well with the measured range precision. This is true for relatively close simulated ranges of 38 m, as well as for emulated target ranges of 880 m. The superposition of WGN considers only the sensitivity limit for the short-range target of the measurement system (quantization noise) and is not directly due to the influence of the frequency synthesizer.

The results also show that the extracted systematic errors must be an essential part of the modeling using the method presented in Section II to estimate the weighting of phase noise and systematic errors in the modeling. In summary, it was confirmed by measurement that the modeling of the two central effects (phase noise and systematic influences) optimally represents the reality in this setup.

VII. CONCLUSION

In this paper, a new model was presented that realistically predicts the range correlation and range precision of radar systems distorted by phase noise and systematic errors. Experimental verification using an analog fiber optical link as delay line allowed emulation of radar targets up to several hundreds of meters to evaluate range-dependent effects.

The analog fiber optical link approach can be extended to include attenuating components to simulate a full-scale radar system while maintaining the reproducibility of the results. The model is modular and allows for considering additional imperfections such as systematic errors up to second-degree polynomials and further distortions. With this modeling approach, the framework was created to model a realistic digital twin of radar systems to simulate, analyze, and predict the feasibility of novel phase distortion compensation methods in the future. This includes coherent radar systems, where range correlation dominates, as well as incoherent radar systems, such as localization or tracking in spatially distributed transceivers, where uncorrelated phase noise is very important.

REFERENCES

[1] E. Rubiola, *Phase Noise and Frequency Stability in Oscillators*. Cambridge, U.K.: Cambridge Univ. Press, 2009.

[2] N. Da Dalt and A. Sheikholeslami, *Understanding Jitter and Phase Noise: A Circuits and Systems Perspective*, 1st ed. Cambridge, U.K.: Cambridge Univ. Press, 2018, doi: 10.1017/9781316981238.

[3] Y. Donnelly and M. P. Kennedy, "Prediction of phase noise and spurs in a nonlinear fractional-N frequency synthesizer," *IEEE Trans. Circuits Syst. I, Reg. Papers*, vol. 66, no. 11, pp. 4108–4121, Nov. 2019, doi: 10.1109/TCSI.2019.2925181.

[4] F. Herzel, A. Ergintav, and Y. Sun, "Phase noise modeling for integrated PLLs in FMCW radar," *IEEE Trans. Circuits Syst. II, Exp. Briefs*, vol. 60, no. 3, pp. 137–141, Mar. 2013, doi: 10.1109/TCSII.2013.2240852.

[5] P. Tschapek, G. Körner, A. Hofmann, C. Carlowitz, and M. Vossiek, "Phase noise spectral density measurement of broadband frequency-modulated radar signals," *IEEE Trans. Microw. Theory Techn.*, vol. 70, no. 4, pp. 2370–2379, Apr. 2022, doi: 10.1109/TMTT.2022.3148311.

[6] K. Thurn, R. Ebelt, and M. Vossiek, "Noise in homodyne FMCW radar systems and its effects on ranging precision," *IEEE MTT-S Int. Microw. Symp. Dig.*, 2013, pp. 1–3, doi: 10.1109/MWSYM.2013.6697654.

[7] R. Ebelt, D. Shmakov, and M. Vossiek, "The effect of phase noise on ranging uncertainty in FMCW secondary radar-based local positioning systems," in *Proc. 9th Eur. Radar Conf.*, 2012, pp. 258–261.

[8] S. Scheiblhofer, S. Schuster, M. Jahn, R. Feger, and A. Stelzer, "Performance analysis of cooperative FMCW radar distance measurement systems," *IEEE MTT-S Int. Microw. Symp. Dig.*, 2008, pp. 121–124, doi: 10.1109/MWSYM.2008.4633118.

[9] F. Herzel, H. J. Ng, and D. Kissinger, "Modeling of range accuracy for a radar system driven by a noisy phase-locked loop," in *Proc. 47th Eur. Microw. Conf.*, 2017, pp. 1369–1372, doi: 10.23919/EuMC.2017.8231107.

[10] S. Scherr, S. Ayhan, B. Fischbach, A. Bhutani, M. Pauli, and T. Zwick, "An efficient frequency and phase estimation algorithm with CRB performance for FMCW radar applications," *IEEE Trans. Instrum. Meas.*, vol. 64, no. 7, pp. 1868–1875, Jul. 2015, doi: 10.1109/TIM.2014.2381354.

[11] R. Krishnan, H. Mehrpouyan, T. Eriksson, and T. Svensson, "Optimal and approximate methods for detection of uncoded data with carrier phase noise," in *Proc. IEEE Glob. Telecommun. Conf.*, 2011, pp. 1–6, doi: 10.1109/GLOCOM.2011.6133627.

[12] G. Sauvage, "Phase noise in oscillators: A mathematical analysis of leeson's model," *IEEE Trans. Instrum. Meas.*, vol. 26, no. 4, pp. 408–410, Dec. 1977, doi: 10.1109/TIM.1977.4314586.

[13] A. Chorti and M. Brookes, "A spectral model for RF oscillators with power-law phase noise," *IEEE Trans. Circuits Syst. I, Reg. Papers*, vol. 53, no. 9, pp. 1989–1999, Sep. 2006, doi: 10.1109/TCSI.2006.881182.

[14] N. J. Kasdin, "Discrete simulation of colored noise and stochastic processes and 1/f alpha; power law noise generation," *Proc. IEEE*, vol. 83, no. 5, pp. 802–827, May 1995, doi: 10.1109/5.381848.

[15] Y. Lisong, C. Xiaolong, and W. Jiali, "A practical simulation method for generating phase noise of oscillators," in *Proc. 2nd Int. Conf. Meas., Inf. Control*, 2013, vol. 01, pp. 132–136, doi: 10.1109/MIC.2013.6757932.

[16] G. V. Klimovitch, "Near-carrier oscillator spectrum due to flicker and white noise," in *Proc. IEEE Int. Symp. Circuits Syst.*, 2000, vol. 1, pp. 703–706, doi: 10.1109/ISCAS.2000.857192.

[17] D. Dhar, P. T. M. van Zeijl, D. Milosevic, H. Gao, and A. H. M. van Roermund, "Modeling and analysis of the effects of PLL phase noise on FMCW radar performance," in *Proc. IEEE Int. Symp. Circuits Syst.*, 2017, pp. 1–4, doi: 10.1109/ISCAS.2017.8050525.

[18] P. Tschapek, G. Körner, P. Fenske, C. Carlowitz, and M. Vossiek, "A novel approach for modeling and digital generation of RF signals distorted by bandlimited phase noise," *IEEE J. Microwaves*, 2022, doi: 10.1109/JMW.2022.3188166.

[19] S. Lanzisera and K. S. J. Pister, "Burst mode two-way ranging with Cramer-Rao bound noise performance," in *Proc. IEEE Glob. Telecommun. Conf.*, 2008, pp. 1–5, doi: 10.1109/GLOCOM.2008.ECP.170.

[20] F. Herzel, D. Kissinger, and H. J. Ng, "Analysis of ranging precision in an FMCW radar measurement using a phase-locked loop," *IEEE Trans. Circuits Syst. I, Reg. Papers*, vol. 65, no. 2, pp. 783–792, Feb. 2018, doi: 10.1109/TCSI.2017.2733041.

[21] M. C. Budge and M. P. Burt, "Range correlation effects in radars," in *Proc. Rec. IEEE Nat. Radar Conf.*, 1993, pp. 212–216, doi: 10.1109/NRC.1993.270463.

[22] S. M. Kay, *Fundamentals of Statistical Signal Processing*. Englewood Cliffs, NJ, USA: Prentice-Hall, 1993.

[23] S. Schuster, S. Scheiblhofer, and A. Stelzer, "The influence of windowing on bias and variance of DFT-based frequency and phase estimation," *IEEE Trans. Instrum. Meas.*, vol. 58, no. 6, pp. 1975–1990, Jun. 2009, doi: 10.1109/TIM.2008.2006131.

[24] A. Demir, "Phase noise and timing jitter in oscillators with colored-noise sources," *IEEE Trans. Circuits Syst. I, Fundam. Theory Appl.*, vol. 49, no. 12, pp. 1782–1791, Dec. 2002, doi: 10.1109/TCSI.2002.805707.

[25] A. J. Hymans and J. Lait, "Analysis of a frequency-modulated continuous-wave ranging system," *Proc. Inst. Elect. Eng. B, Electron. Commun. Eng.*, vol. 107, no. 34, 1960, pp. 365–372.
[26] A. Menditto, M. Patriarca, and B. Magnusson, "Understanding the meaning of accuracy, trueness and precision," *Accreditation Qual. Assurance*, vol. 12, no. 1, pp. 45–47, Jan. 2007, doi: 10.1007/s00769-006-0191-z.
[27] C. H. Cox, *Analog Optical Links: Theory and Practice*. Cambridge, U.K.: Cambridge Univ. Press, 2004.
[28] C. H. Cox, E. I. Ackerman, G. E. Betts, and J. L. Prince, "Limits on the performance of RF-over-fiber links and their impact on device design," *IEEE Trans. Microw. Theory Techn.*, vol. 54, no. 2, pp. 906–920, Feb. 2006, doi: 10.1109/TMTT.2005.863818.
[29] W. S. C. Chang, Ed., *RF Photonic Technology in Optical Fiber Links*. Cambridge, U.K.: Cambridge Univ. Press, 2002, doi: 10.1017/CBO9780511755729.
[30] O. Llopis, S. Azaizia, K. Saleh, A. A. Slimane, and A. Fernandez, "Photodiode 1/f noise and other types of less known baseband noises in optical telecommunications devices," in *Proc. 22nd Int. Conf. Noise Fluctuations*, 2013, pp. 1–4, doi: 10.1109/ICNF.2013.6579014.
[31] D. Eliyahu, D. Seidel, and L. Maleki, "RF amplitude and phase-noise reduction of an optical link and an opto-electronic oscillator," *IEEE Trans. Microw. Theory Techn.*, vol. 56, no. 2, pp. 449–456, Feb. 2008, doi: 10.1109/TMTT.2007.914640.
[32] Z. Abdallah et al., "Photodiode nonlinear modeling and its impact on optical links phase noise," in *Proc. Eur. Freq. Time Forum*, Jun. 2014, pp. 48–51, doi: 10.1109/EFTF.2014.7331423.
[33] M.- Bibey, F. Deborgies, M. Krakowski, and D. Mongardien, "Very low phase-noise optical links - Experiments and theory," *IEEE Trans. Microw. Theory Techn.*, vol. 47, no. 12, pp. 2257–2262, Dec. 1999, doi: 10.1109/22.808968.

PETER TSCHAPEK received the B.Sc. degree in biomedical engineering from Technische Universität Ilmenau, Ilmenau, Germany, in 2014, and the M.Sc. degree in medical engineering from the Friedrich-Alexander-Universität Erlangen-Nürnberg (FAU), Erlangen, Germany, in 2016. He is currently working toward the Ph.D. degree with the Institute of Microwaves and Photonics (LHFT), FAU. In 2017, he joined BLAU Optoelektronik GmbH, Überlingen, Germany, where he was a Development Engineer in the field of testing and measurement of photonic devices. In 2018, he joined LHFT, FAU. His research interests include radar signal processing, measuring and modeling of phase noise, and microwave photonics.

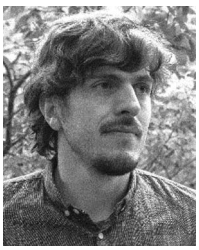

GEORG KÖRNER (Graduate Student Member, IEEE) received the B.Eng. degree in electrical engineering from TH Nürnberg Georg-Simon-Ohm, Nuremberg, Germany, in 2015, and the M.Sc. degree in information and communication technologies from the Friedrich-Alexander-Universität Erlangen-Nürnburg (FAU), Erlangen, Germany, in 2017. From 2014 to 2016, he was a Research Assistant with Siemens AG, Munich, Germany in the field of fiberoptic photonics. After graduation, he joined the Institute of Microwaves and Photonics (LHFT), FAU, in 2017. His research interests include radar signal processing and radar hardware.

CHRISTIAN CARLOWITZ (Member, IEEE) received the Dipl.-Ing. degree in information technology from the Clausthal University of Technology, Clausthal-Zellerfeld, Germany, in 2010. In May 2018, he was awarded the Dr.-Ing. degree from the Friedrich-Alexander-Universität Erlangen-Nürnberg (FAU), Erlangen, Germany for his thesis on wireless high-speed communication based on regenerative sampling. He is currently with the Institute of Microwaves and Photonics, FAU, where he has been leading the Microwave and Photonic Systems Group since 2018. His research interests include the conception, design, and implementation of innovative system architectures for radar and communication frontends at microwave, mm-wave, and optical frequencies. He focuses especially on hardware concepts, and analog and digital signal processing techniques, for ultra-wideband high-speed communication systems, full-duplex mobile communication transceivers, and massive MIMO base stations, as also for ranging and communication with mm-wac systems. Dr. Carlowitz is a member of the IEEE Microwave Theory and Technology Society (MTT-S) and the IEEE MTT-S Technical Committee RF/Mixed-Signal Integrated Circuits and Signal Processing (MTS-15). He is a regular reviewer of IEEE TRANSACTIONS ON MICROWAVE THEORY AND TECHNIQUES and a member of the International Microwave Symposium (IMS) Technical Program Review Committee, and a regular reviewer for several additional international conferences, including EuMW and ICMIM

MARTIN VOSSIEK (Fellow, IEEE) received the Ph.D. degree from Ruhr-Universität Bochum, Bochum, Germany, in 1996. In 1996, he joined Siemens Corporate Technology, Munich, Germany, where he was the Head of the Microwave Systems Group, from 2000 to 2003. Since 2003, he has been a Full Professor with Clausthal University, Clausthal-Zellerfeld, Germany. Since 2011, he has been the Chair of the Institute of Microwaves and Photonics (LHFT), Friedrich-Alexander-Universität Erlangen-Nürnberg (FAU), Erlangen, Germany. He has authored or coauthored more than 300 articles. His research has led to nearly 100 granted patents. His research interests include radar, transponder, RF identification, communication, and wireless locating systems. He is a member of the German National Academy of Science and Engineering (acatech) and the German Research Foundation (DFG) review board. He is a member of the German IEEE Microwave Theory and Technology (MTT)/Antennas and Propagation (AP) Chapter Executive Board and a member of the IEEE MTT Technical Committees MTT-24 Microwave/mm-Wave Radar, Sensing, and Array Systems, MTT 27 Connected and Autonomous Systems (as the Founding Chair), and MTT–29 Microwave Aerospace Systems. He is on the advisory board of the IEEE CRFID Technical Committee on Motion Capture & Localization. He was the recipient of the ten best paper prizes and several other awards. For example, he was awarded the 2019 Microwave Application Award from the IEEE MTT Society (MTT-S) for pioneering research in wireless local positioning systems. Dr. Vossiek is a member of organizing committees and technical program committees for many international conferences and has served on the Review Boards for numerous technical journals. From 2013 to 2019, he was an Associate Editor for IEEE TRANSACTIONS ON MICROWAVE THEORY AND TECHNIQUES.